Non-equilibrium simulations of 4H silicon carbide.

RM Flanagan[1], S Zhao[1], EN Hahn[2], CJ Ruestes[3], CE Wehrehnberg[4], BA Remington[4], MA Meyers[1]

[1] *Department of Mechanical & Aerospace Engineering, University of California, San Diego*
[2] *Los Alamos National Laboratories*
[3] *CONICET and Facultad de Ciencias Exactas y Naturales, Universidad Nacional de Cuyo*
[4] *Lawrence Livermore National Laboratories*

Objective

Using non-equilibrium molecular dynamics simulations, we aim to validate experimental results of laser shock-recovery experiments, where post-mortem high-resolution transmission electron microscopy revealed that above a certain shock threshold, directional amorphous bands form following the formation of stacking faults.

Introduction

Silicon carbide is used in armor[4] and as a semiconductor for high temperature applications[1]. There are over 200 polymorphs, whose structural variations arise from different stacking sequences of Si-C double layers[3, 5]. Figure 1 compares the 3C and 4H SiC structures. In past experiments and simulations, 3C SiC (cubic with periodicity of 3 Si-C double layers) has been shown to undergo a phase transformation to 2H (hexagonal with periodicity of 2 Si-C double layers) when subjected to a pressures ranging from 70 to 140 GPa [7, 8, 11].

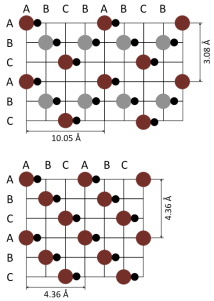

Figure 1: Structural differences between 4H and 3C silicon carbide

4H SiC is under-explored in comparison to 3C SiC. Experiments were performed to explore the behavior of 4H SiC subject to extreme shock loading[12]. Figure 4c shows a high-resolution TEM image of an amorphous domain embedded in crystalline matrix that was shocked at approximately 50 GPa. These experiments motivated simulations of 4H SiC since the formation of directional amorphous bands was unexpected. The goal of these simulations is to verify experimental results while attempting to explore the mechanisms of phase change. Experimental and simulation results show strong agreement.

Method

Simulations of SiC were performed using the LAMMPS package[9]. Initially, a modified Tersoff interatomic potential[2] was considered, but the Vashishta interatomic potential[6] was used since it is better suited for desired pressure regimes. Figure 2 compares selected values of elastic constants produced by both potentials, illustrating how the modified Tersoff potential behaves unreliably at pressures greater than 35 GPa.

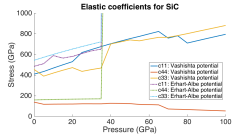

Figure 2: Comparing selected elastic constants calculated using different potential functions

Shock Data

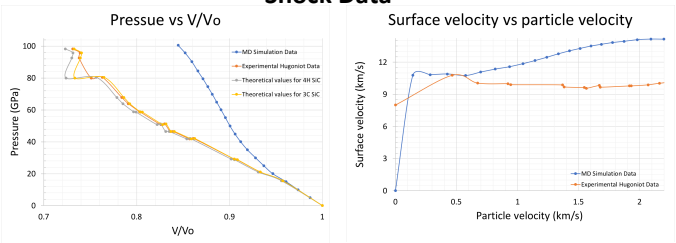

Figure 3: Comparing Hugoniot values between experiment [10] and simulation. The apparent shift between simulation and experimental data is likely due to the simulation's interatomic potential, which estimates a significantly higher bulk modulus than the polymorph used in experiments.

Formation of Amorphous Bands After Shock

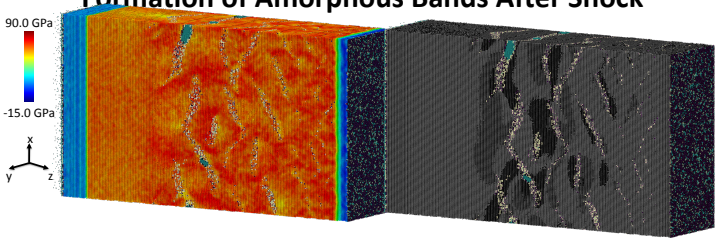

Figure 4a: Visualization of longitudinal stress (left) and defect formation (right) 6.0 ps after shock. At this time, stacking faults and lattice rotation have begun to form, leading to the nucleation of amorphous phases. The lattice rotation is shown by the grey contours in the left figure. Amorphous regions are shown in teal. Stacking faults are multicolored and are further discussed below.

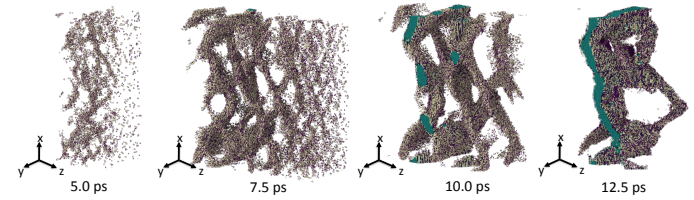

Figure 4b: Evolution of stacking faults during shock. As SiC experiences shear stress, stacking faults form, shown in purple and yellow. Once enough stacking faults form, this leads to a localized phase change which initially seemed amorphous (teal). Upon further investigation, results show that some long range order exists in these spots. The change in volume due to phase transformation leads to lattice rotation, which leads to further stacking faults and phase change until equilibrium is reached.

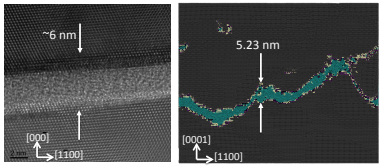

Figure 4c: Comparison between experimental shock recovery TEM image and MD simulation. Experiments were performed at a shock pressure of around 50 GPa while simulations underwent a shock pressure of close to 90 GPa. Although these values differ significantly, it is important to note that the MD results were skewed, likely due to an increased bulk modulus included in the interatomic potential. Qualitatively, direction amorphous bands due to the formation of stacking faults are still observed in both experiment and simulation.

Method, continued

Shock conditions were produced using a controlled piston along the [0001] axis for consistency with experimental work. Hugoniot shock data was collected and compared to previous experimental data[10]. Figure 3 shows the comparison of these characteristic values. All MD simulation figures were generated using Ovito[12].

Results

Using a controlled piston, we produce a shock wave along the [0001] axis and observe the formation of defects along the basal plane, perpendicular to the shock front. Figure 4a shows the formation of lattice rotation and stacking faults following the shock wave. Figure 4b shows how these defects nucleate to form a seemingly amorphous phase. Shear-driven defects continue to evolve as the shock wave propagates through the system and new phases form, leading to further directional amorphization. As shown in figure 4c, present results agree with experiments[13] where horizontal stacking faults and amorphization are observed following laser shock compression and recovery. Post-mortem high-resolution transmission electron microscopy revealed that above a certain shock threshold, directional amorphous bands are observed in the vicinity of the shock surface. The directionality of the bands tends to show agreement between the simulations and the experiment.

Conclusions

- Formation of directional amorphous bands in the vicinity of the shock surface is supported by both experiment and simulation.
- Examination of individual atoms indicate that silicon and carbon atoms tend to stay coordinated in the amorphous phase.
- This phenomenon may be analogous to the transformation of 3C SiC to 2H SiC at high shock pressures.
- Early results show that what seems to be an amorphous phase may partially be nanograins of other silicon carbide solid phases. Further study is being performed to identify these phases and verify their existence.

References

1. Casady, J. B., and R. W. Johnson. *Solid-State Electronics* 39, no. 10 (1996): 1409–22.
2. Erhart, Paul, and Karsten Albe. *Physical Review B* 71, no. 3 (2005): 35211.
3. Fisher, G. R., and P. Barnes. *Philosophical Magazine Part B* 61, no. 2 (1990): 217–36.
4. Flinders, Marc, Darin Ray, Angela Anderson, and Raymond A. Cutler. *Journal of the American Ceramic Society* 88, no. 8 (2005): 2217–26.
5. Harris, Gary Lynn. *Properties of Silicon Carbide*. IET, (1995).
6. Vashishta, P., R. K. Kalia, A. Nakano, and J.P. Rino. *Journal of Applied Physics* 101, no. 10 (2007): 103515.
7. Lee, W. H., X. H. Yao, W. R. Jian, and Q. Han. *Computational Materials Science* 98 (2015): 297–303.
8. Lu, Yu-Ping, Duan-Wei He, Jun Zhu, and Xiang-Dong Yang. *Physica B: Condensed Matter* 403, no. 19–20 (2008): 3543–46.
9. S. Plimpton. | Comp Phys, 117, 1-19 (1995).
10. Marsh, S.P. *LASL Shock Hugoniot Data.* (1980).
11. Shimojo, Fuyuki, Ingvar Ebbsjö, Rajiv K. Kalia, Aiichiro Nakano, Jose P. Rino, and Priya Vashishta. *Physical Review Letters* 84, no. 15 (2000): 3338–41.
12. Stukowski, A. *Modelling and Simulation in Materials Science and Engineering* 18, no. 1 (2010): 15012.
13. Zhao, S. C.E. Wehrehnberg, and B.A. Remington. Silicon Carbide Laser Shock Experiments. Unpublished Raw Data. (2016).